Silicon Photonic Phase Controlled Opto-Optic Beam Steering

Adam Helmy, Hiva Shahoei, Mason Tuller, Mitchell A. Thornton, and Duncan L. MacFarlane

Department of Electrical and Computer Engineering
The Bobby B. Lyle School of Engineering
Southern Methodist University
Dallas, Texas

Abstract— We consider the interaction of coherent light beams at the intersection of waveguides on a photonic integrated circuit. We find the relative phase between the beams steers or switches the beams to different outputs. This effect has much in common with phased array antenna beam steering in free space [1-4]; however, the integrated architecture studied here provides a variety of new applications and utility. One exemplary geometry is the intersection of two perpendicular waveguides. Here, C-band waveguides are made of silicon with silicon dioxide cladding. The relative phase between two input waves entering the intersection from the West and the South controls whether the output wave exits either to the North ($\frac{3\pi}{2}$ radians) or East ($\frac{\pi}{2}$ radians). Higher contrast between the two outputs can be achieved with the addition of a thin 45-degree, 100-nanometer trench across the center of the intersection. Experiments with the trench design indicate a -2.5 dB insertion loss and a 23 dB extinction ratio when applying TE polarized light on both inputs. As might be expected from a phase-dependent effect, there is often a pronounced polarization signature to the effect. Using one TE and one TM source does not enable beam steering as the corresponding electrical fields are approximately orthogonal. Given two nearly TE polarized inputs of the same power, the high power output remains TE polarized but due to the slight difference in polarization states of the two inputs, the low power output is rotated to be nearly TM. Applications include on-chip photonic switching and routing, photonic filtering and signal processing, and photonic sensors [5-9]. This effect offers an interpretation of the photon bunching that occurs upon the simultaneous arrival of two indistinguishable photons at a beamsplitter [10].

1. INTRODUCTION

That coherent waves scattering from adjacent apertures will interfere in a manner that enables the steering of the resultant beam is well known [1], This effect has been demonstrated using integrated photonics to steer a beam emitted into free space from an array of apertures [2-4]. In this paper, we show that in an integrated photonic architecture, this phased array can lead to opto-optic switching; the phase of one beam can control the routing of the composite beam. This new application is the topic of this paper.

Consider the intersection of two waveguides on a photonic integrated circuit (PIC) as shown in Fig. 1. The commercial simulation package, Lumerical [11] is used to model the scenario. Fig. 1a shows a single 193.4 THz (1550 nm) input passing relatively undisturbed from the South port to the North. Figures 1b – 1d show coherent inputs from the West and South with different relative phases. For in-phase inputs(1b), the outputs to the North and East are relatively balanced. For a phase shift of -90 degrees, the output is dominantly to the North (1c). For a phase shift of +90 degrees, the output is dominantly to the East (1d).

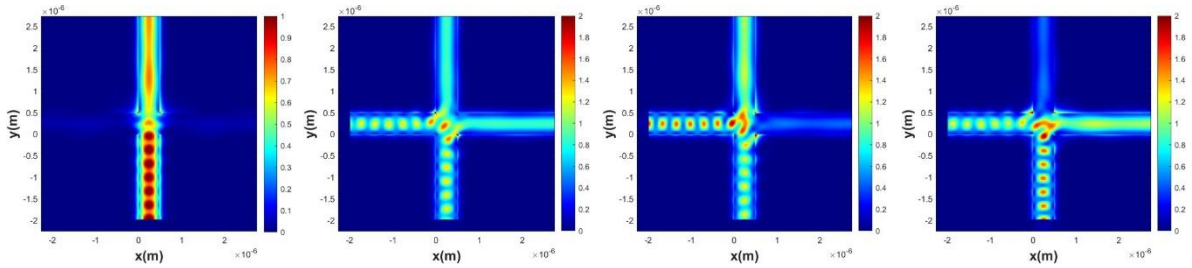

(a) (b) (c) (d)

Figure 1. The intersection of two single-mode (480 nm x 220 nm) Si/SiO2waveguides. Fig. 1a shows a single 193.4 THz (1550 nm) input passing relatively undisturbed from the South port to the North. Figures 1b – 1c show coherent inputs from the West and South with different relative phases. For in-phase inputs(1b), the outputs to the North and East are relatively balanced. For a phase shift of -90 degrees, the output is dominantly to the North (1c). For a phase shift of +90 degrees, the output is dominantly to the East (1d).

The geometry of the devices in this paper allow for extremely compact and scalable integrated photonic logic. The only limitations on minimum footprint are those of the 480 nm x 220 nm Si platform itself and the path length required to achieve a specific phase shift. Unlike traditional amplitude modulators based on phase modulation, this design is not limited by bend radius and naturally allows for a scalable grid structure that could be the basis of a reconfigurable 2D waveguide mesh network [7-9].

The remainder of this paper discusses the physics, context, and applications of this effect.

2. MODELING WITH HUYGEN'S PRINCIPLE

The Huygens-Fresnel principle governs the majority of geometries where diffraction arises, and an excellent treatment of the theory is covered in Born and Wolf [12]. The structure of the well-known integral, the Huygens' construction, that governs diffraction,

$$U(P) = \iint_S A\frac{e^{ik(r_0-s)}}{r_0 - s}K(\chi)dS \tag{1}$$

Is that of a convolution between the field $K(\chi)$ across the surface, S, and the delta function response of a point source, often called a Green's function.

In Figure 2, the discretized construction used to model the interference within the 480 nm x 480 nm intersection is shown. We place point sources of equal amplitude along the West and South Input apertures, and calculate the summations of the fields from each source, taking into account the phase of each component based on the optical path length between points.

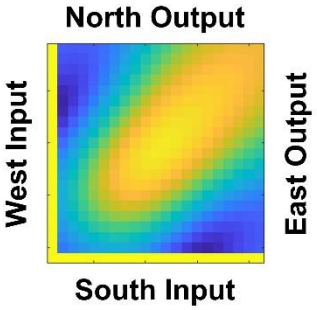

Figure 2. Huygens-Fresnel modeling at the intersection of two waveguides. The West and South input apertures are each lined with an array of spherical sources, and their interference in the 480 nm x 480 nm intersection is plotted.

Thus, the field at an arbitrary grid point $E(x,y)$ is the phase weighted sum of each of the sources. Those from the West Input comprise the first triple summation, and those from the South Input comprise the second.

$$E(x,y) = \sum_{n,x,y=1}^{21} e^{j*\left(S_{Grid}*\frac{2\pi}{\lambda}n_{eff}*\sqrt{x^2+(n-y)^2}+\Delta\phi\right)} + \sum_{n,x,y=1}^{21} e^{j*S_{Grid}*\frac{2\pi}{\lambda}n_{eff}*\sqrt{(n-x)^2+y^2}} \tag{2}$$

Note, in particular, the $\Delta\phi$ phase term is the relative phase difference between the West and South inputs. To generate the nine diffraction cases shown in Figure 3, the $\Delta\phi$ phase term is swept from 0 to 360 degrees. As expected, the center of mass of the field is steered across the diagonal of the intersection.

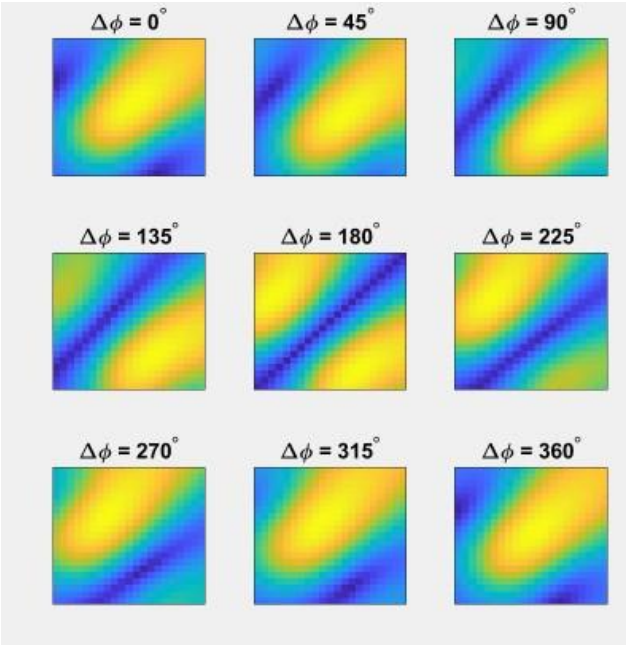

Figure 3. Interference of the arrays of spherical sources as the relative phase of the West and South apertures is swept through 360 degrees.

3. MODELING WITH COMMERCIAL DESIGN PACKAGES

We use two common, well-accepted commercial platforms to inform us of the wave propagation behavior across the intersection of two 480 nm wide x 220 nm tall Si waveguides. The cladding present in the PIC is

SiO_2. These waveguide dimensions and material system are common for Foundry-based Silicon Photonics, and provide single-mode operation at 193.4 THz (1550 nm).

Lumerical FDTD is a commercial software package that employs the Finite-Difference Time-Domain method [13]. The simulation domain is discretized into a structured mesh of rectangular cells, and Maxwell's equations are solved directly in the time domain. The electric and magnetic fields are computed at each point in space and time as the wave propagates. This time-stepping approach captures both transient and steady-state behavior, making it well suited for broadband simulations as it can handle a wide range of frequencies simultaneously. However, FDTD requires fine temporal and spatial resolution, which can result in significant computational costs, especially for large structures with fine features. The results in Fig. 1 were calculated using Lumerical FDTD. In general, the following settings were used in this work: Simulation regions are 5 um x 5 um with 2 um height; Mesh set to auto non-uniform with a 'mesh accuracy' of 8 (highest setting); the minimum mesh step is 0.00025 um; Perfectly matched layer boundary conditions and the Colorbar scale is set to 2.

In addition to modeling with Lumerical FDTD, Ansys HFSS (High Frequency Structure Simulator) was used to confirm the results. Ansys HFSS uses the Finite Element Method to solve Maxwell's equations in the frequency domain. Good agreement was obtained between the two commercial packages, and this adds to the confidence of the results presented herein.

The Lumerical calculated contrast ratio between the maximum, in-phase output power and the minimum, out-of-phase output power for the intersections presented thus far is approximately 3.9 dB with an insertion loss of -1.1 dB. Improved performance can be achieved with the addition of a thin, 45-degree, 100 nm SiO_2 trench across the center of the intersection [14, 15]. Lumerical calculations of beam-steering at an intersection with the trench are shown in Figure 4. In Figure 4a, there is a -90 degree phase shift between the West and South inputs and in Figure 4b, there is a +90 degree phase shift between the West and South inputs. A higher contrast of 11.4 dB between the two outputs is calculated with the addition of a thin 100-nanometer trench. The insertion loss in this case is -1.5 dB.

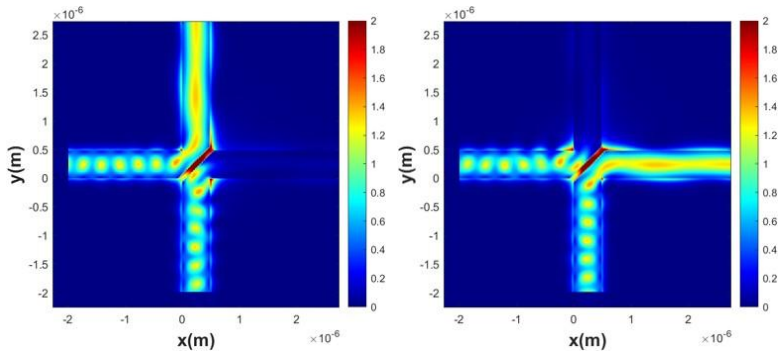

Figure 4. Lumerical calculation of the Beam-steering at an intersection with a thin 100 nm SiO2 trench; in (a) and (b), there are -90 degree and +90 degree phase shift between the West and South inputs respectively.

In Figure 5 is plotted the output powers on the North and East outputs as the phase on the West input is swept. The quantitative switch between the two outputs is clearly shown.

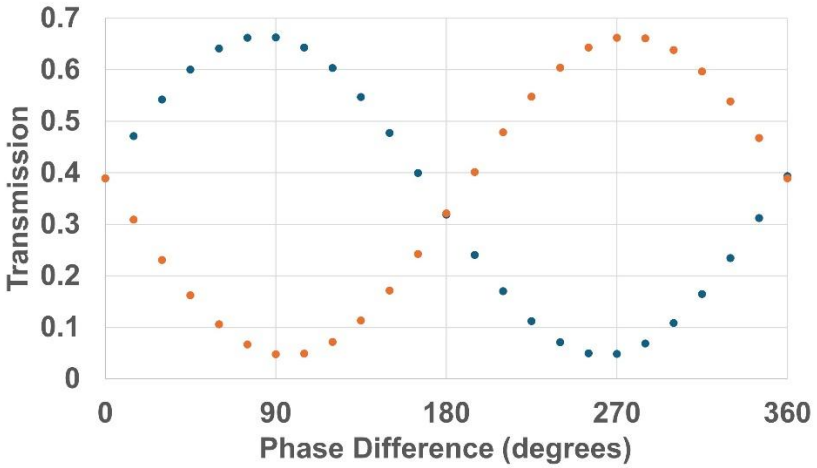

Figure 5. A plot of the output powers on the North and East outputs as the phase on the West input is swept. The quantitative switch between the two outputs is clearly shown.

As might be expected from a phase-dependent effect, there is often a pronounced polarization signature to the effect. Using one TE and one TM source does not enable beam steering as the corresponding electrical fields are approximately orthogonal. Given two nearly TE polarized inputs of the same power, the high-power

output remains TE polarized, but due to the slight difference in polarization states of the two inputs, the low-power output is rotated to be nearly TM.

4. EXPERIMENT

The silicon-photonic integrated circuit (Si-PIC) used in the experiments was designed in-house and fabricated at AIM Photonics using its Multi-Project Wafer (MPW) offering [16]. The layout of the Si-PIC is shown in Figure 6a, and a close-up of the section-under-test is shown in Figure 6b. An SEM (Scanning Electron Micrograph) of the intersection with the trench is shown in Figure 6c. The silicon dioxide cladding has been etched away in the SEM, leaving the 480 nm by 220 nm silicon waveguides and the 100 nm trench exposed. The Si-PIC was packaged by attaching a Polarization-Maintaining Fiber (PMF) array to the relevant edge couplers.

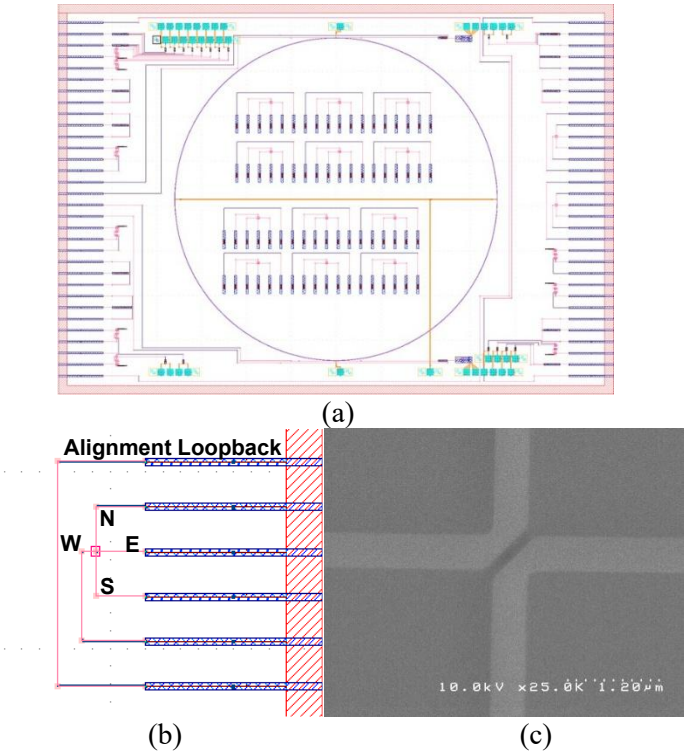

Figure 6. The layout of the Si-PIC is shown in Figure 6a, and a close-up of the section-under-test is shown in Figure 6b. An SEM (Scanning Electron Micrograph) of the intersection with the trench is shown in Figure 6c. The silicon dioxide cladding and trench fill has been etched away.

The beam steering of the intersection was verified using the experimental configuration shown in Figure 7. The output of a C-band tunable external cavity laser was divided into two approximately equal components using a one-by-two fiber splitter. Polarization controllers PC-1 and PC-2 maximize the coupling onto the chip and ensure the polarization is matched at the two input ports of the intersection. Power meters PM-1 and PM-2 simultaneously monitor the two outputs of the intersection.

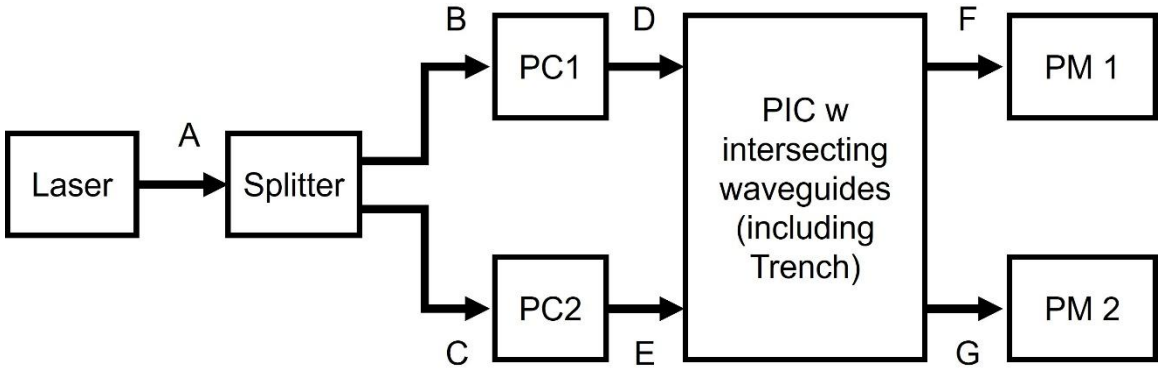

Figure 7. The beam steering of the intersection was verified using the experimental configuration shown in Figure E-2. The output of a C-band tunable external cavity laser was divided into two approximately equal components using a one-by-two fiber splitter. Polarization controllers PC-1 and PC-2 maximize the coupling onto the chip and ensure the polarization is matched at the two input ports of the intersection. Power meters PM-1 and PM-2 simultaneously monitor the two outputs of the intersection.

In Figure 8 is a time trace of the output powers as measured by power meters PM-1 and PM-2. As

expected, the traces mirror each other. When PM-1 is high, PM-2 is low, and vice versa. We interpret these results as beam steering caused by random phase variations induced on the input fibers and waveguides leading into the intersection. The observed extinction ratio is measured to be 23 dB.

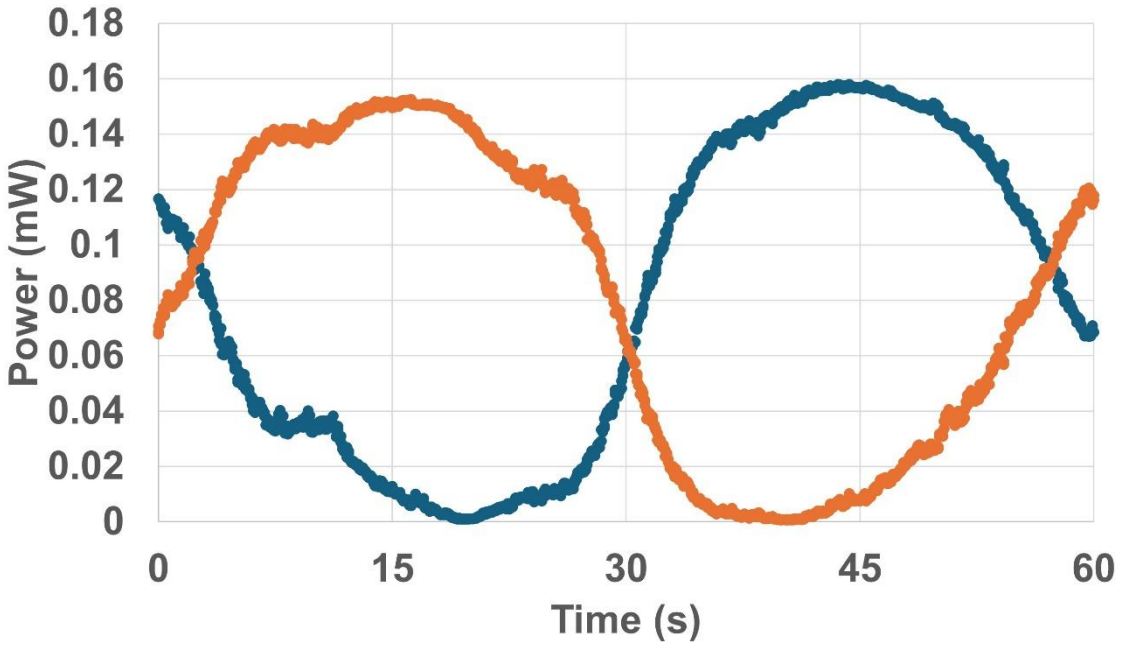

Figure 8. Simultaneous temporal traces of the output powers as measured by power meters PM-1 and PM-2.

5. Applications, Classical and Quantum

This paper has explored the routing of two coherent signals interacting at the intersection of two integrated waveguides. The resultant beam, a superposition of the two inputs, is directed to one or the other output waveguide depending on the phase between the two inputs.

With no trench in the intersection, the Lumerical calculated contrast ratio between the maximum in-phase output power and the minimum out-of-phase output power for the intersections is approximately 3.9 dB with an insertion loss of -1.1 dB. A higher contrast of 11.4 dB between the two outputs is calculated with the addition of a thin, 100-nanometer trench. This case has a slightly higher insertion loss of -1.5 dB. Experiments with the trench design indicated 2.5 dB insertion loss and a 23 dB contrast ratio when applying TE polarized light to both inputs.

While the physics of this work is the same as a phased array antenna, the finite number of waveguides and their close proximity are discretized as the input-output relationship. A phase-dependent logical operation follows wherein the North output waveguide is either high or low depending on the input phase. The East output wave guide is the inverse logic level. The compact nature of the intersection implies that a field of gates can be fabricated on a single chip, and reasonably scaled optical logic can be realized.

Phase control of the input beam can be achieved in several ways, depending on the material platform of the PIC. In the silicon photonic platform, a temporally slow thermal process can be engineered by incorporating doped silicon heaters that run parallel to the waveguides. In other PIC systems that use electro-optic materials, the phase can be controlled with the voltage applied directly to the input waveguides.

When two individual, indistinguishable photons arrive at a beamsplitter, it is experimentally observed that the two photons exit together along the same output path [10]. The results presented here offer a perspective on this quantum effect, called photon bunching.

Acknowledgment

A. Helmy is a Templeton Fellow at SMU and thanks them for making this research possible.

REFERENCES

1. Braun, K. F. "Electrical oscillations and wireless telegraphy," Nobel Lecture, Dec. 11, 1909. [Online], available: https://www.nobelprize.org/uploads/2018/06/braun-lecture.pdf.
2. Gagino M., A. Millan-Mejia, L. Augustin, K. Williams, E. Bente, and V. Dolores-Calzadilla, “Integrated optical phased array with on-chip amplification enabling programmable beam shaping,” Sci. Rep., Vol. 14, No. 9590, 2024. Accessed on: July 30, 2025, doi: 10.1038/s41598-024-60204-5, [Online].
3. Yi Y., D. Wu, V. Kakdarvishi, B. Yu, Y. Zhuang, and A. Khalilian, “Photonic integrated circuits for an optical phased array,” Photonics, Vol. 11, No. 3, 243, 2024. Accessed on: July 30, 2025, doi: 10.3390/photonics11030243, [Online].

4. Wu Y., R. Jiang, Y. Wang, and W. Fu, “Hybrid integrated silicon nitride optical phased array with phase calibration for two-dimensional beam steering,” Opt. Express, Vol. 33, No. 5, 11123-11137, 2025. Accessed on: July 30, 2025, doi: 10.1364/OE.539929, [Online].
5. MacFarlane, D. L., J. Tong, C. Fadadia, V. Govindan, L. R. Hunt and I. Panahi, "Extended lattice filters enabled by four-directional couplers," *Appl. Opt.*, Vol. 43, No. 33, 6124-6133, 2004. Accessed on: May 27, 2025, doi: 10.1364/AO.43.006124, [Online].
6. MacFarlane, D. L., M. P. Christensen, A. E. Nagdi, G. A. Evans, L. R. Hunt and N. Huntoon, "Experiment and Theory of an Active Optical Filter," *IEEE J. Quantum Elect*., Vol. 48, No. 3, 307-317, 2011. Accessed on: May 27, 2025, doi: 10.1109/jqe.2011.2174615, [Online].
7. Pérez D., I. Gasulla, P. Das Mahapatra, and J. Capmany, “Principles, fundamentals and applications of programmable integrated photonics,” Adv. Opt. Photonics, Vol. 12, No. 3, 709-786, 2020. Accessed on: August 1, 2025, doi: 10.1364/AOP.387155, [Online].
8. Lyke J. C., C. G. Christodoulou, G. A. Vera, and A. H. Edwards, “An introduction to reconfigurable systems,” Proc. IEEE, Vol. 103, No. 3, 291-317, 2015. Accessed on: August 1, 2025, doi: 10.1109/JPROC.2015.2397832
9. Pérez-López D., A. López-Hernández, A. Macho, P. Das Mahapatra, and J. Capmany, “Towards field-programmable photonic gate arrays,” *Proceedings of Smart Photonics and Optoelectronic Integrated Circuits XXII*, San Francisco, USA, February 2020.
10. Beugnon, J., M. P. A. Jones, J. Dingjan, B. Darquié, G. Messin, A. Browaeys and B. Grangier, "Quantum interference between two single photons emitted by independently trapped atoms," *Nat.*, Vol. 440, No. 7085, 779-782, Dec. 1909. Accessed on: May 27, 2025, doi: 10.1038/nature04628, [Online].
11. ANSYS, “What is Finite-Difference Time-Domain (FDTD)?,” Ansys Blog, Jan. 23, 2024 [Online]. Available: https://www.ansys.com/blog/what-is-fdtd. Accessed on: July 19, 2025.
12. Born M. and Wolf E., *Principles of Optics: Electromagnetic Theory of Propagation* Interference and Diffraction of Light, “Chapter VIII: Elements of the Theory of Diffraction,” pp370-458, Pergamon Press, Sixth Edition, 1980.
13. Kunz K. S. and R. J. Luebbers, *The Finite Difference Time Domain Method for Electromagnetics*, CRC Press 1993.
14. Huntoon N. R., M. P. Christensen, D. L. MacFarlane, G. A. Evans, C.S. Yeh, “Integrated photonic coupler based on frustrated total internal reflection,” Appl. Opt., Vol. 47, No. 30, 5682-5690, 2008. Accessed on: July 25, 2025, doi: 10.1364/AO.47.005682, [Online].
15. Shahoei, H., I. G. Achu, E. J. Stewart, U. Tariq, W. V. Oxford, M. A. Thornton, and D. L. MacFarlane, “Silicon photonics 2x2 trench coupler design and foundry fabrication,” Appl. Opt., Vol. 61, No. 16, 4927-4931, 2022. Accessed on: May 27, 2025, doi: 10.1364/AO.453464, [Online].
16. Bowers, J., R. Alferness, R. L. Clark, D. Coolbaugh, L. Kimerling, T. L. Koch, “American institute for manufacturing integrated photonics (AIM Photonics),” *Proceedings of IEEE Avionics and Vehicle Fiber-Optis and Photonics Conference (AVFOP)*, Santa Barbara, USA, November 2015.